ELSEVIER

Contents lists available at ScienceDirect

# Biosensors and Bioelectronics

journal homepage: www.elsevier.com/locate/bios





# Real-time monitoring of single-cell secretion with a high-throughput nanoplasmonic microarray

Yen-Cheng Liu<sup>a</sup>, Saeid Ansaryan<sup>a</sup>, Xiaokang Li<sup>a,b,c</sup>, Eduardo R. Arvelo<sup>a,d</sup>, Hatice Altug<sup>a,\*</sup>

- a Institute of Bioengineering, École Polytechnique Fédérale de Lausanne (EPFL), Lausanne, 1015, Switzerland
- <sup>b</sup> Ludwig Institute for Cancer Research, University of Lausanne, Agora Center, 1005, Lausanne, Switzerland
- <sup>c</sup> Department of Oncology, Centre Hospitalier Universitaire Vaudois (CHUV), 1011, Lausanne, Switzerland
- d Department of Electrical and Computer Engineering, University of Wisconsin-Madison, Madison, WI, 53706, USA

#### ARTICLE INFO

#### Keywords: Single-cell analysis High throughput Nanoplasmonic sensor Label-free biosensing Microwell array

#### ABSTRACT

Proteins secreted by cells play significant roles in mediating many physiological, developmental, and pathological processes due to their functions in intra/intercellular communication and signaling. Conventional endpoint methods are insufficient for understanding the temporal response in cell secretion process, which is often highly dynamic. Furthermore, cellular heterogeneity makes it essential to analyze secretory proteins from single cells. To uncover individual cellular activities and the underlying kinetics, new technologies are needed for real-time analysis of the secretomes of many cells at single-cell resolution. This study reports a high-throughput biosensing microarray platform, which is capable of label-free and real-time secretome monitoring from a large number of living single cells using a biochip integrating ultrasensitive nanoplasmonic substrate and microwell compartments having volumes of ~0.4 nL. Precise synchronization of image acquisition and microscope stage movement of the developed optical platform enables spectroscopic analysis with high temporal and spectral resolution. In addition, our system allows simultaneous optical imaging of cells to track morphology changes for a comprehensive understanding of cellular behavior. We demonstrated the platform performance by detecting interleukin-2 secretion from hundreds of single lymphoma cells in real-time over many hours. Significantly, the analysis of the secretion kinetics allows us to study cellular response to the stimulations in a statistical way. The new platform is a promising tool for the characterization of single-cell functionalities given its versatility, throughput and label-free configuration.

## 1. Introduction

In recent years, single-cell analysis has become an extraordinarily powerful approach to revealing cell heterogeneity, a phenomenon that provides insights for precise drug development, personalized therapies, and curing intractable diseases, like cancer (Lawson et al., 2018; Wang and Bodovitz, 2010). Monitoring cellular secretion from living single cells is of particular importance since it unveils the distinct cellular responses to external stimuli (e.g., small chemicals (Dura et al., 2015), hypoxia (Olive and Aquino-Parsons, 2004)), which is critical for cell typing and biomarker discovery. The secretion of cytokines, which are a broad range of small proteins (interleukins, interferons, etc.), represents an important role in cell signaling among various cellular responses (Makridakis and Vlahou, 2010). Such a process is in particular highly time dependent and heterogeneous, and the kinetics can reflect multiple

physiological activities, for instance, landmark in immune responses (Sojka et al., 2004). When immune cells are stimulated, various types of cytokines are secreted in a dynamic manner to activate the immune effector responses and regulate immune cell maturation. Therefore, capturing this behavior with high enough temporal resolution is crucial for understanding the basic cell functionalities or the efficacy of a treatment (Bucheli et al., 2021). Furthermore, studying cellular functional responses of the transient cytokine release at the single-cell level helps to characterize the intercellular communication network (Thurley et al., 2018). The analysis of these molecules requires an ultrasensitive and precise methodology due to their minute amount and nanoscale sizes. Although conventional approaches, such as the enzyme-linked immune absorbent spot (ELISpot) and fluorescence-activated cell sorting (FACS), can provide reliable information of specific biomolecules with high specificity, they provide only end-point results, which

E-mail address: hatice.altug@epfl.ch (H. Altug).

 $<sup>^{\</sup>ast}$  Corresponding author.

overwrites the dynamic process of cell secretion, and thus impairs real-time measurements for kinetic studies. Moreover, their qualitative nature fails to provide quantitative insights into cellular processes.

For analysis of protein secretion, multiple efforts have been made. Ma et al. reported a single-cell chip with immobilized capture antibodies forming barcode patterns, and observed highly functional heterogeneity in the analysis of cytokines from single cytotoxic T lymphocytes (Ma et al., 2011). Han et al. used nanowell arrays and glass slide with capture antibodies to monitor the Th1-skewed cytokines (IFN- $\gamma$ , IL-2, and TNF $\alpha$ ) from human CD3+ T cells over incubation and measurement cycles to obtain time-dependent profile of single-cell monitoring with the resolution of 2 h (Han et al., 2012). However, analyzing the secreted proteins at a single-cell level mainly relies on fluorescence bioassays. Although fluorescence assays can reach the required sensitivity for measuring single-cell secretion, the use of fluorescence tags limits the applications due to the tedious labelling process and compromises the time resolution for measuring kinetics with complex handling/washing steps. Therefore, it is in critical need for dynamic living cell analysis without using molecule tags for signal interrogation.

Label-free biosensing technologies have emerged to tackle the challenges in label-based assays in the past two decades. Among the various types of signal transduction mechanisms (electrical (Pui et al., 2013; Shin et al., 2017), optical (Khansili et al., 2018), acoustic (Chang et al., 2014; Länge et al., 2003), magnetic (Gaster et al., 2011), etc.), optical biosensors have the advantages of wide applicability, sensitivity, and the capability of device integration for advanced lab-on-a-chip (LOC) systems. Recent developments in micro/nanofabrication have further paved a wider path for nanophotonics, the study of light in the sub-wavelength scale, and its interaction with nanostructures (Monticone and Alu, 2017). Given the strong light-matter interaction, nanophotonic structures enable the detection of molecules much smaller than the wavelength of light in a label-free and non-invasive manner (Soler et al., 2020; Yesilkoy et al., 2019; Zanchetta et al., 2017). Nevertheless, as powerful and flexible as the label-free nanophotonic biosensors, their exploitation for living cell analysis is in its infancy. Li et al. showed that nanoplasmonic sensors can offer sensitivity to detect secretion at the single-cell level, but with measurements limited to one cell at a time (Li et al., 2018). In recent years, some studies have reported the monitoring of living single cells with biosensors based on dielectric photonic crystals (Juan-Colás et al., 2018) and localized surface plasmons (Zhu et al., 2020) at a limited throughput with only few tens of cells. Therefore, label-free sensing platforms that can fulfill the requirements of sensitivity, high throughput, and high temporal resolution are vet to be developed.

In high-throughput single-cell analysis systems, another consideration is the isolation of individual cells into separate compartments for avoiding signal disturbances and crosstalk among multiple cells. Thanks to the development of microelectromechanical systems and microfluidic technology, the handling and analysis of single cells have become feasible and accessible. Studies have demonstrated the compartmentalization of single cells with various microfluidic techniques including microwells (Rettig and Folch, 2005; Wood et al., 2010; Zhou et al., 2020), microdroplets (Brouzes et al., 2009; Mazutis et al., 2013), and hydrodynamic microtrap devices (Bithi and Vanapalli, 2017; Carlo et al., 2006; Kimmerling et al., 2016), which are proven to be effective and easy to handle. However, the single-cell distribution depends mainly on passive cell loading that lacks a sufficient cell positioning accuracy, resulting in a relatively low singularity yield. Recently, the yield has been greatly improved by adopting active cell loading with dielectrophoresis (DEP) (Taff and Voldman, 2005; Wu et al., 2017) or optoelectronic tweezers (OET) (Hsu et al., 2010; Wu, 2011). Nonetheless, the above approaches require rather complicated chip fabrication, and the use of electrodes limits their applications. Single cell handling components that are easy to use and can be integrated straightforwardly with biosensors are needed to have LOC and micro total analysis systems for comprehensive single-cell analysis.

In this paper, we present a high-throughput and ultrasensitive nanoplasmonic biosensor integrated with microwell compartment arrays for living single cells to achieve label-free and real-time secretome monitoring on a large scale. The nanoplasmonic substrate utilizes gold nanohole arrays (AuNHA), whose spectrum shifts highly sensitively in response to the localized refractive index change upon binding of analytes on its surface. The high-throughput configuration is achieved by precisely synchronizing microscope stage movement and acquisition of spectral images to "scan through" the entire microarray and measure the resonance shifts caused by the secretome release from each cell at high temporal and spectral resolution. In addition to the spectroscopic signal, our system simultaneously acquires optical images of the cells to correlate their morphologies and secretion behaviors. The single cells are dispensed in a deterministic and efficient way by a piezoelectricbased ultralow volume liquid dispensing tool (Hartlmayr et al., 2021; Vallone et al., 2020) into a simple 2D microwell compartment array made of polydimethylsiloxane (PDMS). We demonstrate that our integrated device can extract spatially and temporally resolved single cell secretion sensorgram at high resolution and provide important parameters such as secretion onset, duration, and level. We apply it to detect interleukin-2 (IL-2) secreted by mouse lymphoma cell line EL4 under different treatments. With the stable control of the temperature and humidity and proper composition of the cell medium, the cells are kept alive for monitoring longer than 20 h. We achieved real-time IL-2 secretion analysis of hundreds of single cells in a high-throughput manner, which is essential to construct statistical behavior of secretion kinetics from a certain single-cell group under various biological conditions. The flexibility and simplicity of the single-cell plasmonic microarray make it highly versatile to adapt to and study different cell types and secretomes.

## 2. Experimental section

#### 2.1. Cell culture

EL4 cells (ATCC TIB-39) are cultured in Dulbecco's Modified Eagle Media (DMEM, Gibco, MA, USA) with an additional supplement of 10% FBS (Gibco, MA, USA), 1% penicillin/streptomycin (Gibco, MA, USA), and 10 mM HEPES buffer (Gibco, MA, USA). All cells were incubated at 37  $^{\circ}\text{C}$  in an incubator with 5% CO2, and a confluency of >80% was reached before the single-cell measurements.

## 2.2. Fabrication of the NHA biosensor chip

The gold nanohole array chips were fabricated on a wafer scale using deep-UV lithography technique for the patterning of nanoholes. Fused silica wafers (100 mm diameter, 500 μm thickness, UniversityWafer, Inc.) were cleaned with standard RCA procedure, then deposited with Ti-Au metal films (10 nm Ti + 120 nm Au) using an electron beam evaporator (EVA760, Alliance Concept). Ti layer was employed to promote the adhesion of Au film as Ti is reactive with both the fused silica substrate and the gold layer; moreover, it suppressed the irrelevant surface modes induced by the Au/glass interface. After a post clean with RCA1 procedure to further remove possible polymer residues, the NHAs (200 nm diameter, 600 nm period) were patterned using a 248 nm deep-UV stepper (PAS 5500/300 DUV, ASML). The NHA pattern on Ti-Au films was formed by an ion beam etching system (Ionfab 300 Plus, Oxford Instruments plc), followed by a resist stripping process. A second lithography step to pattern the identification codes for each chip was completed to track the chips further and ensure consistent results. This step was done using a mask-less direct laser writer (MLA150, Heidelberg Instruments) and followed by gold wet etching using an iodine-based gold etchant (TechniEtch™ACI2, Microchemicals GmbH). A waferlevel characterization of the AuNHA showing characteristic parameters on a wafer map is demonstrated in Fig. S1. Next,  $1 \text{ cm} \times 1 \text{ cm}$  dies were separated using a dicing saw (DAD321, DISCO Corporation).

Finally, the photoresist from the second lithography step was removed with a positive photoresist remover solution (MICROPOSIT Remover 1165, Rohm & Haas Electronic Materials LLC) at 70 °C and 15 min of sonication twice. The chips were then stored for future use after the oxygen plasma cleaning for 1 min (Tepla 300, VA TePla America).

#### 2.3. Fabrication of microwell meshes

The microwell mesh membranes (100 µm in diameter, 50 µm in depth) for the confinement of cells were fabricated by a replica molding process with PDMS. A master mold composed of micro posts was first prepared by photolithography process using a direct laser writer (VPG200, Heidelberg Instruments) to pattern the spin-coated positive photoresist (AZ9221, Microchemicals GmbH) followed by a deep reactive Ion etching (Adixen AMS200) on a 4-inch silicon substrate. After the photoresist removal by oxygen plasma (GIGAbatch 360, PVA MPS GmbH), the mold surface was then silanized by the evaporation of Trimethylsilyl chloride (TMCS) to form a passivation layer for the aid of future PDMS release. The mixture of base PDMS (Sylgard 184 silicone, Dow Corning Corp.) and the cross-linker (Sylgard curing agent, Dow Corning Corp.) with the weight ratio of 10:1 was degassed, then poured into the master mold on a spin coater (SCS 6800, Specialty Coating Systems Inc.) to form a thin layer with the thickness around 60 μm. Next, the mold wafer coated with PDMS was cured in an oven at 80 °C for 2 h. Then the cured PDMS was etched using an ICP-based high-density plasma etching system (Advanced Plasma System (APS), SPTS Technologies Ltd.) to reveal the silicon posts, which became microwells when the polymer membranes were peeled from the master mold. The peeled microwell mesh was finally attached to the functionalized AuNHA surface, making an integrated chip ready for the cell secretion analysis.

## 2.4. Biosensor surface functionalization and sensor calibration

The AuNHA biosensor chip was cleaned with acetone, isopropanol, and Milli-Q water consecutively prior to a UV-ozone treatment for 20 min. The chip was then immersed in an ethanolic solution composed of 0.1 mM biotin PEGylated thiol (Biotin-PEG-SH) and 0.9 mM hydroxyl PEG thiol (OH-PEG-SH) (Prochimia Surfaces) in a nitrogen glove box to avoid atmospheric moisture. After 8-12 h of the thiolation process, the chip was rinsed with ethanol, dried with nitrogen gas, and incubated with 0.01% poly-L-lysine (Sigma-Aldrich Chemie GmbH) and 50 μg/mL streptavidin solution (Life Technologies) diluted in phosphate-buffered saline (PBS) for overnight at 4°C. Wash steps of the chip with PBS a few times were done to remove the unbound streptavidin molecules before incubation with biotinylated mouse IL-2 antibodies (Abcam plc.). 20 μg/mL of the antibody was used to react with the streptavidin on the chip surface for 1 h at room temperature, followed by a few times PBS wash steps. After a quick rinse with Milli-Q water and gentle drying with nitrogen gas, the functionalized AuNHA chip was ready to be assembled with the PDMS microwell mesh for cell dispensing to conduct secretion analysis. For the biosensor calibration, we assembled the chip with microfluidic channels and injected standard recombinant IL-2 proteins (Abcam plc.) diluted in PBS at the flow rate of 5  $\mu$ L/min using a syringe pump (PHD ULTRATM, Harvard Apparatus) at various concentrations. The limit of detection (LOD) of the biosensor was defined as LOD =  $3.3\sigma/S$ , where  $\sigma$  is the standard deviation of the response and S is the slope of the calibration curve at lower concentration range. The chip integration configuration and the resulted calibration curve are shown in Fig. S2. Aside from the aforementioned standard functionalization, an additional real-time measurement for the binding of streptavidin and antibody was done to validate the functionalization process. The characterization results are shown in Fig. S3.

## 2.5. Single-cell dispensing with piezoelectric spotter

The ultralow volume liquid spotting system with automated cell

imaging (cellenONE ×1, Cellenion SASU) was implemented to isolate the cells into the microwells. The humidity in the system was controlled at 65%, and the temperature on the sample holder surface was kept at the dew point (15-17 °C depending on the air temperature) to prevent excessive drying. The AuNHA chip with PDMS microwell mesh attached was placed in a chamber slide (μ-Slide 2 Well, ibidi GMBH), and the slide was clamped on the sample holder. Before dispensing the cells, fresh media was spotted into the wells with 1% glycerol added to avoid evaporation. The cell density was diluted to  $2-5 \times 10^5/\text{mL}$  in basal medium for best isolation throughput, and then a mapping step was done to characterize cell sizes and shapes through a few parameters including diameter, circularity, and elongation. With criteria of the parameters set based on the acquired mapping data, single cells meeting the criteria were recognized, isolated, and spotted into the assigned microwells with  $\sim 100\%$  efficiency. The time required for spotting 100 cells is approximately 5 min. After cell dispensing in the wells, the chip was incubated in the system for 10 min for the cells to settle to the bottom. A pre-warmed mixture of cell culture media (DMEM), 0.1% FBS, 500 μM N-acetyl-L-cysteine (NAC), and 2 × insulin-transferrin-selenium (ITS) with either the stimulation cocktail or stimulation + inhibition cocktail was added to the chamber slide to immerse the chip completely and start the stimulation of all spotted cells at the same time. Then the device was moved to the sensing platform for optical measurements.

## 2.6. Optical measurement setup and data processing

The optical measurement consists of the acquisition of spectroscopic images and optical images. The normally incident light from broadband tungsten-halogen lamp filtered by a bandpass filter (central wavelength 860 nm, FWHM 120 nm, Salvo Technologies Inc.) was illuminated on the nanoplasmonic chip. The EOT signal was collected with an objective lens and then split by a dual camera image splitter (TwinCam, Cairn Research) installed onto an inverted microscope (Nikon Ti-U). A 4  $\times$ objective lens (CFI Plan Fluor, NA = 0.13) is used for the binding assay, and a 20  $\times$  objective lens (CFI LWD DL, NA = 0.4) is used for the cell measurement. One of the two beams goes to a spectrometer (Shamrock 303i, Andor, spectral resolution 0.1 nm) and a deep-cooled CCD camera (iKon-M, Andor) with 1024  $\times$  1024 pixels and 13  $\times$  13  $\mu m^2$  pixel size, forming 1D spectroscopic images through a slit opening and a grating of 600 lines mm<sup>-1</sup>. The other beam goes to a monochrome CMOS camera (DS-Qi2, Nikon) with 4908  $\times$  3264 pixels and 7.3  $\times$  7.3  $\mu$ m<sup>2</sup> pixel size as optical images. The data acquisition, real-time analysis, and display were realized through a customized MATLAB graphic user interface. In the interface, stage positions corresponding to the regions near single EL4 cells were defined first. Adjacent to each microwell with a single cell, an empty microwell is allocated as a reference such that the signal from this region without a cell is used to account for the effect of systematic drifts. The spectra were extracted by the interface, and the region-of-interest (ROI) on the spectral images was selected to measure and calculate the resonance peak centroid within a fixed wavelength window (60% peak-to-valley intensity). In the measurement, the spectroscopic image and optical image files were sorted into the corresponding folders for further processing and the calculated temporal sensorgram for multiple ROIs were plotted in real-time. The saved spectroscopic images were analyzed further to construct the spatiotemporal sensorgram, which presents the resonance shift across the slit over time with a spatial resolution of  $\sim$ 0.6  $\mu m$  and a temporal resolution of 2–5 min, depending on the number of stage positions. The data was further upsampled by  $5 \times$  with interpolation for both time and position axis, and smoothed with Lowess smoothing and median smoothing to remove signal noise for plotting.

#### 3. Results and discussion

## 3.1. Configuration of the high-throughput dual imaging platform

The nanoplasmonic single-cell microarray platform provides the capability of high-throughput analysis by integrating microscope stage control and data file sorting. A schematic illustration of the system configuration is depicted in Fig. 1. The biosensor chip consists of two attached parts: a  $1 \times 1$  cm<sup>2</sup> plasmonic nanohole array substrate for monitoring of secretion response, and a 50 µm thick PDMS layer containing microwell arrays, which isolates the single cells and minimizes crosstalk by neighbouring cells. For the measurements, the biosensor chip is placed on an inverted microscope and illuminated with a collimated light source with normal incidence. The transmitted light enters an objective and is split via a beam splitter: one beam is used to track the cell morphology with optical imaging, while the other beam is used to generate the sensor's spectrum. This dual imaging scheme provides insights to the cell morphology and its correlation with the secretion behavior as a function of time. For time-resolved optical imaging of the cells, a CCD camera is used. For the spectral analysis, the beam goes through a slit and then is dispersed by a grating and recorded in realtime by a second CCD camera coupled to a spectrometer. The spectroscopic imaging gives only 1D information of optical wavelength (horizontal axis,  $\lambda$ ) across the illuminated area of the NHAs through the slit opening (vertical axis, Y) at a given position in X-axis. In order to obtain 2D spectral information in both X and Y axis, we scanned the chip with a motorized stage. A user interface was designed with MATLAB to synchronize the stage movement and the image acquisition into the corresponding folders in a specific region, allowing the scanning of over  $\sim$ 100 cells in a single experiment at a temporal resolution of  $\sim$ 4 min. With post-processing, time-resolved 2D plasmonic spectral information were extracted from multiple regions over the sensor.

The biosensing principle is based on the extraordinary optical transmission (EOT) phenomenon on the AuNHA and the strong

dependence of the EOT resonance spectrum to the local refractive index changes. When the secreted proteins bind to specific antibodies functionalized on the sensor surface, the refractive index variation in the vicinity results in a redshift of the EOT resonance ( $\Delta\lambda$ ) in the wells containing a secreting cell. On the other hand, the empty wells without the single cells do not show such a resonance shift. In the microarray, we keep every other row empty and use these wells as references to correct the systematic signal drift caused by environmental conditions. By tracking the spectral shifts continuously from time-resolved spectral images, we obtain the sensorgram to monitor the secretion dynamics from multiple single cells. This read-out scheme benefits from the configuration of the plasmonic substrate featuring nanoholes that are patterned over the entire chip surface. In this way, each point on the sensor acts as a sensing element and gives the flexibility to define ROI freely, irrespective of the cell position. Compared to more complex nanostructures which require high-resolution nanofabrication methods such as electron beam lithography, we manufactured our substrates by a high-throughput manufacturing process based on deep-UV lithography and patterned nanohole structures over the entire four-inch wafer in a uniform manner. This fabrication method reduces the manufacturing cost and enables disposable sensor chips.

The cell compartmentalization on the biochip requires no complex apparatus and sophisticated fluid control. It consists of a thin PDMS microwell mesh membrane attached to the AuNHA substrate (Fig. 2a), and the integrated biochip is immersed in the culturing medium (Fig. 2b) on a standard microscope slide with chambers. The upper left and upper right panel of Fig. 2c show the layout design and optical microscope images of the microwell mesh, which is composed of  $3\times 3$  blocks with each block containing  $10\times 10$  microwells that have the diameter and spacing of  $100~\mu m$ . The volume of each microwell is 0.39~nL.

To load single cells in the microwell array, we used a piezoelectric ultralow-volume liquid dispenser with automated imaging for single-cell isolation to ensure a deterministic cell dispensing. The volume of a

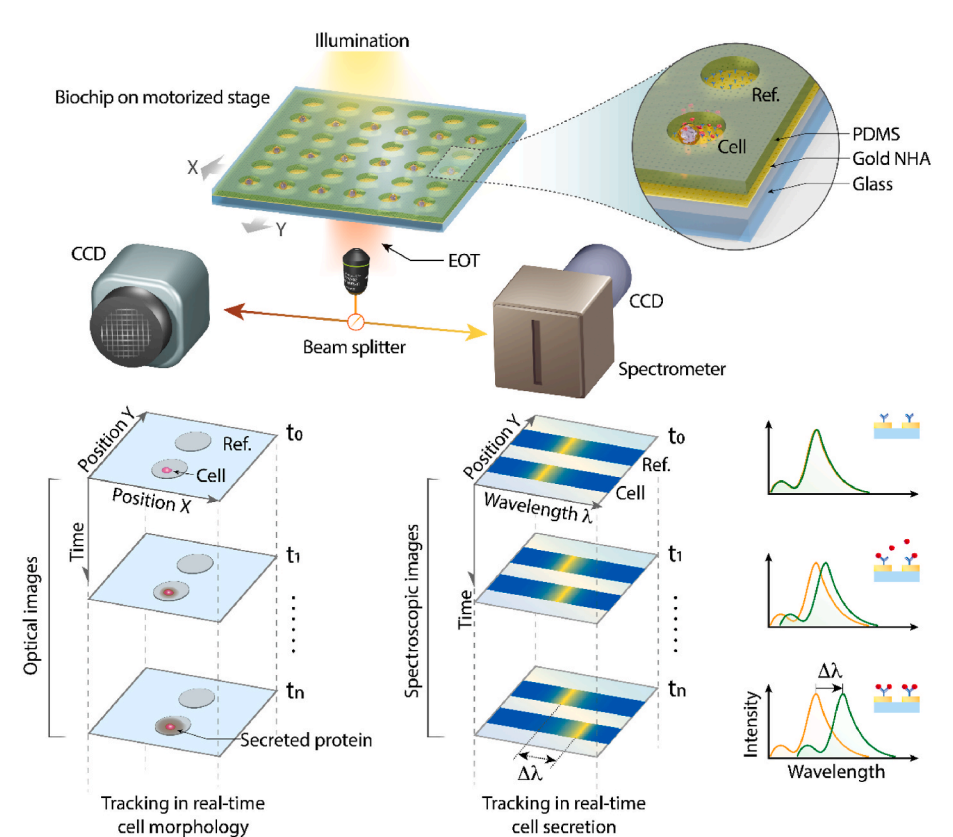


Fig. 1. Schematic representation of the integrated biochip and the measurement system for acquiring both spectroscopic and bright-field optical microscope images. The collected light goes through a beam splitter and the resulting two beams are analyzed simultaneously in real-time with a spectrometer to monitor cell secretion dynamics by tracking EOT resonance peak through spectroscopic images, and with a CCD camera to observe cell morphology through optical images. The stage movement and the acquisition of the images are automated and precisely synchronized. The acquired real-time data are analyzed with a custom-made MATLAB user interface for tracking the binding events from large numbers of microwells. The binding events of secreted analytes by the cells on the functionalized nanohole array surface can be quantified in a label-free manner by measuring the resonance shift ( $\Delta\lambda$ ) dynamically from the acquired time-resolved spectroscopic images. The biochip is utilized in a way that each well containing a cell has an adjacent empty well as a reference.

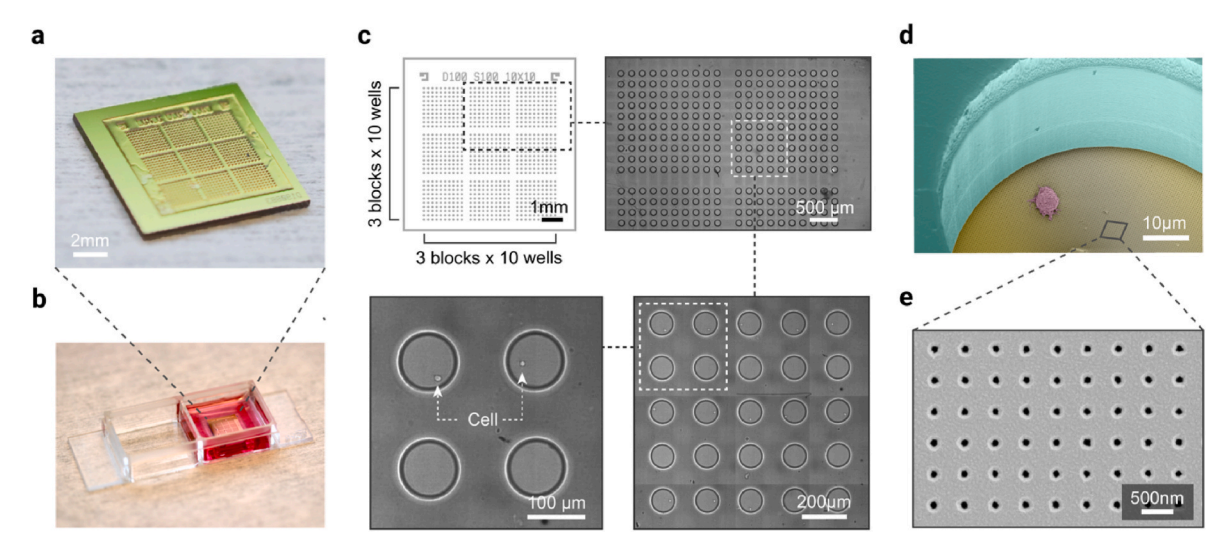


Fig. 2. Configuration of the biochip with microwell array design for single-cell secretion analysis. (a) The picture of the integrated biochip consisting of a nano-plasmonic AuNHA substrate with PDMS microwell mesh attached to it. (b) The picture of the chamber slide for measurement with the biochip immersed in a specific cell medium. (c) Illustration of the microwell array, including the layout design of the well array consisting of  $3 \times 3$  blocks and  $10 \times 10$  wells in each block (upper left), optical image of marked region from the layout image under bright-field microscope with  $4 \times$  objectives (upper right), stitched image of  $5 \times 5$  microwells with  $20 \times$  objectives (lower right), and a zoomed-in  $2 \times 2$  microwell image showing single EL4 cells dispensed in the wells (lower left). (d) Colored SEM image of a single EL4 cell in the microwell, attached to the AuNHA substrate. (e) Zoomed-in SEM image of the uniformly distributed gold nanoholes with 200 nm diameter and 600 nm period.

single droplet formed by the piezoelectric nozzle can go as low as 300 pL, and the system can complete the loading of 100 cells in  $\sim$ 5 min. The humidity and temperature of the spotting system are controlled to maintain the sample surface at the dew point, thus preventing the dispensed liquid from drying out and causing stress on the cells. The dispensed cells lying on the nanohole array are contained in the microwells as shown in the optical microscope image in Fig. 2c (lower right and lower left panel) and the digitally colored scanning electron microscopy (SEM) image in Fig. 2d.

## 3.2. Binding assay and scanning demonstration

To demonstrate the high-throughput dual imaging scheme and the construction of time-resolved 2D resonant shift information, we performed a binding assay on a microarray of  $10 \times 10$  microwells with 100 μm diameter. The piezoelectric spotter was used to dispense IL-2 specific antibodies and bovine serum albumin (BSA) into PDMS microwells on biotin PEGylated thiol and streptavidin-coated AuNHA surface. As shown in Fig. 3a, biotinylated IL-2 antibodies were dispensed in half of the wells at regular intervals of every other well. The other half of the microwell array was dispensed with biotinylated BSA, which is expected to block the surface from adsorbing molecules. These wells are used as references to correct the background signal. After overnight incubation at 4°C following the antibody and BSA spotting, the biochip was washed with PBS. For the binding assay, we utilized a microfluidic flow cell covering the microwells to perform the tests with small sample volumes (Fig. S4) in a stably controlled manner. Recombinant IL-2 proteins at a concentration of 250 ng/mL were introduced at a flow rate of 10  $\mu$ L/ min.

For the binding assay, we used a 4  $\times$  objective lens to capture optical images from 10  $\times$  10 wells and spectroscopic images of 10 wells in a row with a slit width of 50  $\mu m.$  In order to collect the time-resolved 1D spectroscopic images of all the wells, their positions were pre-defined and the motorized stage automatically scanned in the X direction (Fig. 3b) over the entire array in a periodic fashion. The acquired spectroscopic data were then processed to construct a 2D resonance shift information of the full microarray as a function of time using the centroid tracking method (see Experimental section). This procedure results in a temporal resolution of 30s for a given well in the current

microarray configuration. Fig. 3b shows the corresponding 2D spectral plot of the microwell array with two types of surface functionalization: anti-IL2 functionalized positive wells and BSA-blocked control. The color represents the resonance shift after IL-2 injection with respect to the initial value (scale indicated by the color bar below). All the positive wells show obvious redshift, while the control wells had negligible shifting. This indicates that the recombinant IL-2 mostly binds to the antibody-functionalized wells rather than to the BSA-blocked wells, thus verifying our biosensor capable of detecting the target analyte with specificity. A time-lapse video of the 2D spectral plot at various time points further provides a clear visualization of spectral shifts in the wells over time (Movie S1). The real-time 1D spectroscopic images at one slit position are used to plot spatiotemporal sensorgrams along the Y-axis as shown in Fig. 3c. Here, the left panel represents the corresponding optical image of the selected five wells, and the brighter area indicates the fixed slit position (along the X axis). By analyzing the resonance peaks on every pixel over time from the spectroscopic images, the resonance shift is obtained in the form of color changes (scale indicated by the color bar). In this sensorgram, the redshift signal in positive wells started to appear at around 20 min in all the three wells, matching the IL-2 solution injection time. On the other hand, the very slight variation of resonance in the control wells proves that there is very limited well-towell cross-contamination, making the single-cell analysis reliable without the concern of signal interference by adjacent wells.

Supplementary data related to this article can be found at https://do i.org/10.1016/j.bios.2021.113955.

By selecting the ROIs on the spatiotemporal sensorgram over the Y axis (indicated by colored arrows in Fig. 3c) and averaging their spectral shift information, we can obtain the conventional sensorgram curves resolved only in time. The curves in Fig. 3e show similar red-shifting levels for the three positive wells and similarly low shifting amounts for the two control wells. Fig. 3d shows the temporal sensorgram of the entire microarray averaged over 50 positive wells and 50 control wells with three times of standard deviation indicated as the shaded area for each curve (see inset for a clearer visualization). The low level of variation shows that the functionalized biochip is rather homogeneous in response to the presence of the analytes. This binding assay on the microarray demonstrates that our platform can scan over a large area to analyze multiple wells in a high-throughput manner.

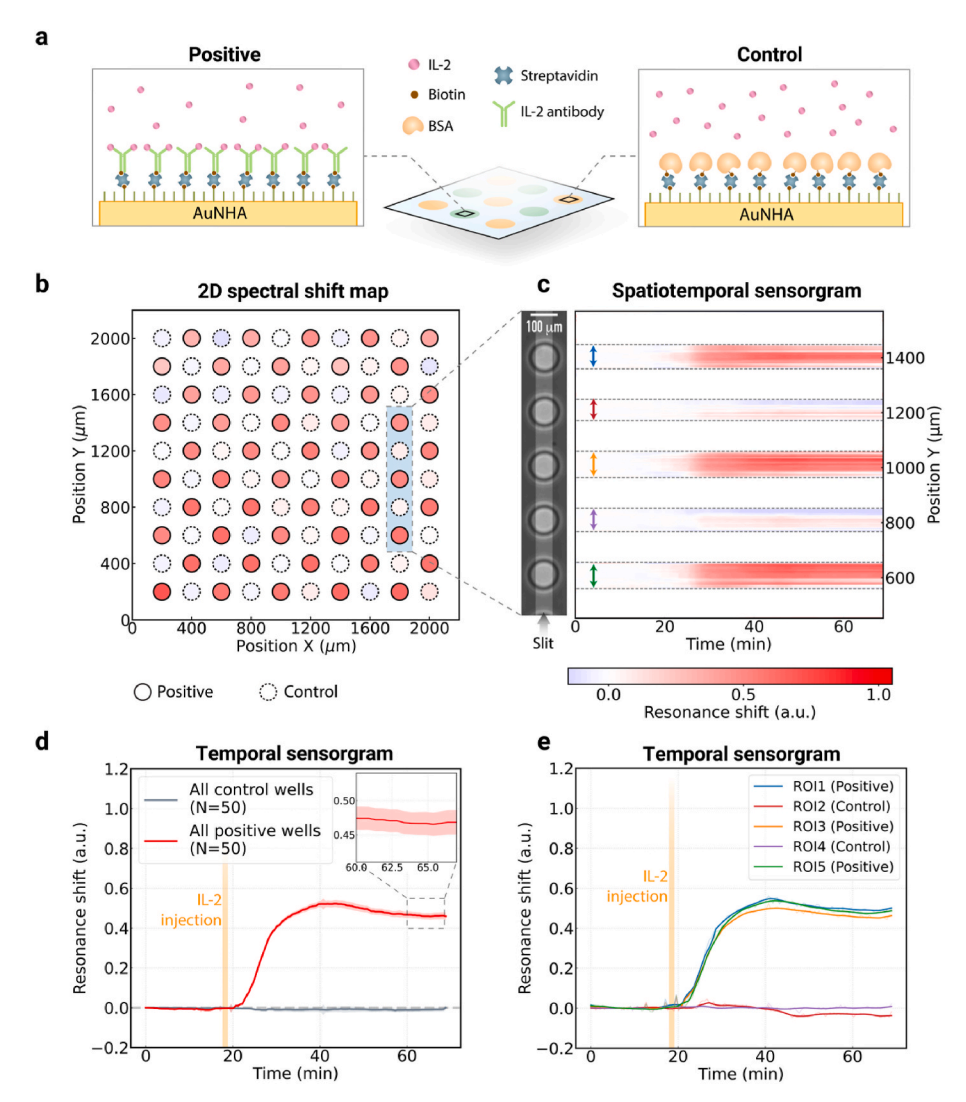


Fig. 3. Demonstration of a large-area microarray spectroscopic scanning for performing highthroughput and real-time bioassay with molecular specificity. (a) Surface functionalization for the AuNHA sensor. The gold surface modified with PEGylated alkanethiol self-assembled monolayer with functional group of biotin is linked with biotinylated IL-2 antibody through streptavidin in half of the wells. In the other half of the wells, IL-2 antibodies are replaced by biotinylated BSA to block the surface and they are used as a control group. (b) End-point 2D spectral shift map of all the wells in a  $10 \times 10$ microarray extracted from time-resolved 1D spectroscopic images that are obtained by stage scanning. The shift values are calculated based on the resonance wavelength difference between the average of T = 5-15 min and T = 50-65 min. Anti-IL2-functionalized wells (positive) are circled with solid lines, and BSAblocked wells (control) are circled with dashed lines. (c) Spatiotemporal sensorgram of five selected microwells analyzed with time-resolved 1D spectroscopic image stacks. The left panel shows the optical image of these wells with the fixed slit position indicated by the brighter area. (d) The temporal sensorgram of the entire microarray averaged over 50 positive wells and 50 control wells. The shaded area represents three times of the standard deviation, and the solid line represents the mean value of all the curves. (e) Temporal sensorgram of the five selected wells obtained from ROIs shown in panel (c) with colored arrows.

## 3.3. Real-time IL-2 secretion detection with spatiotemporal analysis

We next performed the real-time and high-throughput analysis of the cytokine secretion from single EL4 cells. EL4 mouse lymphoma cells serve as a good model for our experiment since they produce IL-2 cytokines only in response to a defined chemical stimulus (Farrar et al., 1980), making it ideal for the verification of our new platform. For a given experiment, we scanned two blocks of microwell arrays consisting of  $10 \times 10$  wells with a configuration of each well containing a cell inside has an adjacent empty well as a reference. We collected data from hundreds of cells from multiple different experiments. Half of the cells were treated 30 min with a stimulation cocktail (phorbol 12-myristate 13-acetate (PMA) + ionomycin) (Miyajima et al., 2015) prior to the measurements. The other half were treated 30 min with both the stimuli and inhibitor prior to the measurements as the control group. The inhibitor cocktail of Brefeldin A and Monensin block intracellular protein transport processes, resulting in the accumulation of secreted proteins in the cells (Schuerwegh et al., 2001).

For the cell assay, we used a  $20\times$  objective lens to acquire the bright field optical images of  $4\times4$  wells and the spectroscopic images of  $3\times1$  wells with a slit width of 10  $\mu m$ . Prior to the measurements, stage positions were defined manually such that the slit is  $\sim\!20~\mu m$  from the cell. With the poly-L-lysine used to stabilize anchoring of the cells on the sensor surface, we observed that cell displacement is minimal in the wells during the measurement, providing similar distances between the

cells and the slit for comparable measurements from cell to cell. The limited displacements can be seen in the supplementary movies of three representative cells in both experimental and control group (Movie S2-S7). To collect the time-resolved 1D spectroscopic images of all the cells, the motorized stage scanned repeatedly in both X and Y directions over the entire microarray and the images were sorted into the corresponding folder for real-time and post analysis. The acquired spectroscopic data were processed to construct 2D resonant shift information of all the cells as a function of time at a temporal resolution of  $\sim\!\!4$  min. At the same time, the optical images of the corresponding wells were visualized for simultaneous monitoring of the cell condition.

Supplementary data related to this article can be found at https://do i.org/10.1016/j.bios.2021.113955.

The continuous measurements of IL-2 secretion from EL4 cells were performed for more than 20 h. Fig. 4a shows the spatiotemporal sensorgram of a representative cell in the microarray. The redshift signal is directly attributed to the secretion and in situ capture of the IL-2 cytokine. Snapshots of a cell-containing well at five time points from T=0 to T=20 h with a 5-h interval are shown in Fig. 4b, in which the slit location is indicated as the brighter area. The color-coded ROIs overlapping with the slit correspond to the ROI areas that are marked in the spatiotemporal sensorgram. Close-up images of the cells for each snapshot are shown in the bottom row. By averaging the spectral shift information over the Y-axis within the three selected ROIs on the spatiotemporal sensorgram (indicated by colors in Fig. 4a and b), we

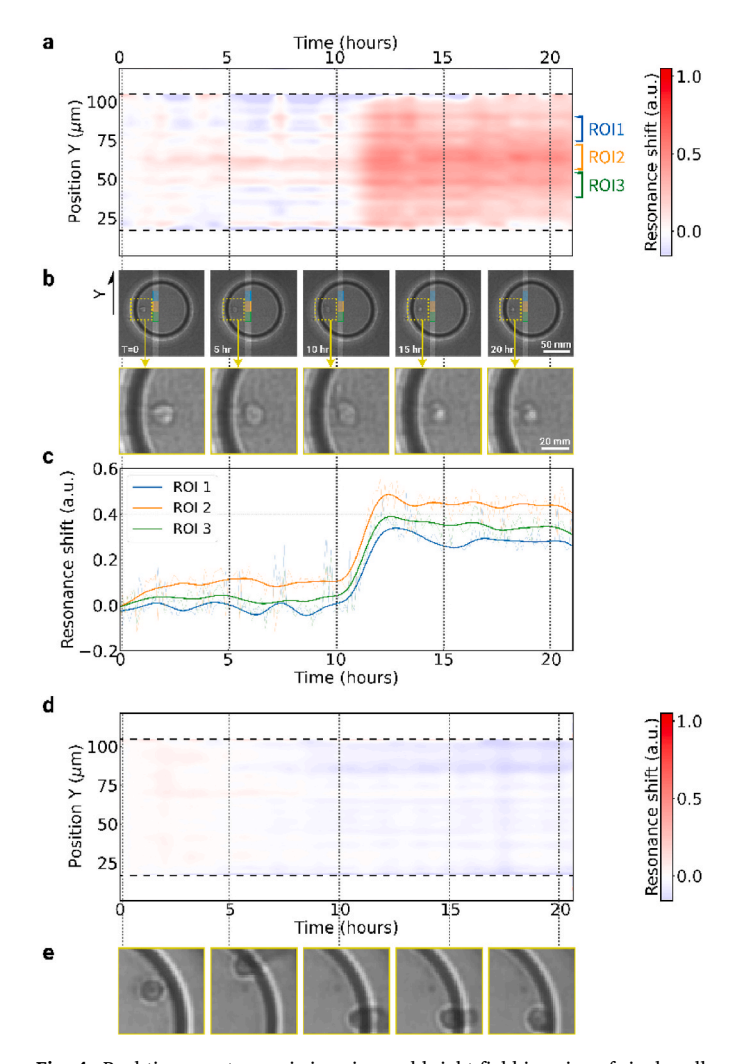


Fig. 4. Real-time spectroscopic imaging and bright-field imaging of single-cell secretion. (a) Spatiotemporal sensorgram of a single EL4 cell secreting IL-2 cytokine upon chemical stimulation. It is constructed by analyzing the resonance peak information from time-resolved 1D spectroscopic images along the Y axis corresponding to the spectrometer slit. The horizontal dashed lines are the boundaries of the microwell. (b) Snapshots of one EL4 cell in the microwell at various time points (top) and the zoom-in views of the cell (bottom). Each optical image is connected with a dashed line to the sensorgrams at the corresponding time points. The fixed slit position is indicated by the brighter area in the top images. (c) Three temporal sensorgram curves obtained by averaging the resonance shift information along the Y-axis within the ROIs indicated in Fig. 4a-b with the same color. (d) Spatiotemporal sensorgram of IL2 secretion for a single EL4 cell from a control group exposed to both chemical stimulation and inhibition. (e) Zoomed-in snapshots of one EL4 cell in the control group in microwell at various time points.

plot the corresponding temporal sensorgram curves in Fig. 4c. Both the spatiotemporal sensorgram and temporal sensorgram show a distinguishable signal increase around 10–12 h, and the signal levels off afterward. The real-time recording of the optical images of the cell is shown in Movie S2. The timing when the cell activity slows down coincides with the secretion signal increase in both sensorgram (Fig. 4a and c). This suggests that the cell underwent a large extent of protein release after stimulation, which also triggered its apoptosis. (Munn et al., 1995; Wesselborg et al., 1993). We also observed larger signal around the region closest to the cell which can be attributed that the functionalized antibodies on the sensor around the cell capture effectively the IL-2 cytokine upon the secretion.

The control experiment is carried out by exposing the cells in both the stimulation cocktail and a protein transport inhibitor cocktail. The

result of one representative cell in this group is shown in Fig. 4d. The spatiotemporal sensorgram remained light-colored across the entire experiment, indicating a subtle amount of IL2 secretion. The temporal sensorgram also showed a correspondingly flat curve (Fig. S5). The snapshots of the cell (Fig. 4e) indicate that the cell is viable (Movie S8). This specific cell has been one of the most active cells ( $\sim$ 3% of all measured cells) showing slightly more displacement. The absence of resonance response in the negative control group indicates that our biosensing platform is selective for IL-2 detection and responds to no other proteins in the culture medium.

Supplementary data related to this article can be found at https://do i.org/10.1016/j.bios.2021.113955.

#### 3.4. Single-cell secretion profiling of EL4 cells

The high-throughput capability of our plasmonic microarray platform enables us to investigate the real-time IL-2 secretion response from a large number of single EL4 cells. To illustrate this feature, we analyzed single cells from an experimental group (with stimuli) and a control group (with stimuli + inhibitor) in multiple experiments. For each cell, a temporal sensorgram curve is obtained by averaging the spectral shift on the spatiotemporal sensorgram over the axis of slit direction within a 20-pixel ROI having the shortest distance to the cell. This temporal sensorgram curve is used to characterize the dynamics of the protein secretion with the following three parameters indicated in Fig. 5a: onset time, secretion duration, and the maximum signal level. Those parameters reflect the kinetic process of functional response to external stimulation from individual cells, and can be used for determining potent cell activation in relation to the immune cell applications (Sojka et al., 2004).

In the experimental and the control groups, we studied 150 and 65 cells, respectively. The criteria for secreting cells is set to be the ones having positive resonance shift level higher than three times of the standard deviation of the baseline noise. As shown in Fig. 5b, the percentage of cells with a secretion signal in the experimental group is significantly higher than in the control group, 38.0% versus 13.8%. The fact that some cells in the control group still showed secretion signal may be due to the time difference in effectiveness between the stimulation and the inhibition, that is, some control cells may be stimulated and start to secrete cytokine before the inhibition takes place. The 3D scatter plot in Fig. 5c provides further insights into these two groups. Here, the three quantitative characteristics of the secretion curve are presented as the axes. As can be seen, there is a distinguishable difference in the dot distribution on all the axes. The control group (blue dots) is mainly localized around the origin of the coordinates, while the experimental group (red dots) showed a wider distribution in all three categories.

Separate histograms (Fig. 5d–f) show the distribution of cells in terms of each parameter and profile the dynamics of the IL-2 secretion from the EL4 cell line. Fig. 5d shows the comparison of the onset time between the two groups. The cells in the experimental group show the signal onset at an early time but also extend to later stages, indicating that cells respond to stimuli in different manners due to the cell heterogeneity. On the other hand, cells in the control group showed signal onset only at an early time. This suggests that IL-2 was only secreted in the beginning of the measurement, before the inhibitor became effective and blocked the protein transport processes.

Fig. 5e and f shows the comparison of secretion duration and the secreted level. As before, we can observe different behavior between the cells in the experimental and the control groups. For the control group, the limited numbers of secreting cells had a shorter duration of secretion and a lower secretion level. Such a phenomenon can also be attributed to the inhibitor's effect, which stopped the ongoing IL-2 secretion, thus keeping the duration not longer than 6 h and the secreted IL-2 at a lower amount. For the experimental group, although they tended to secrete IL-2 for a shorter duration, some of the cells still continued to secrete over a

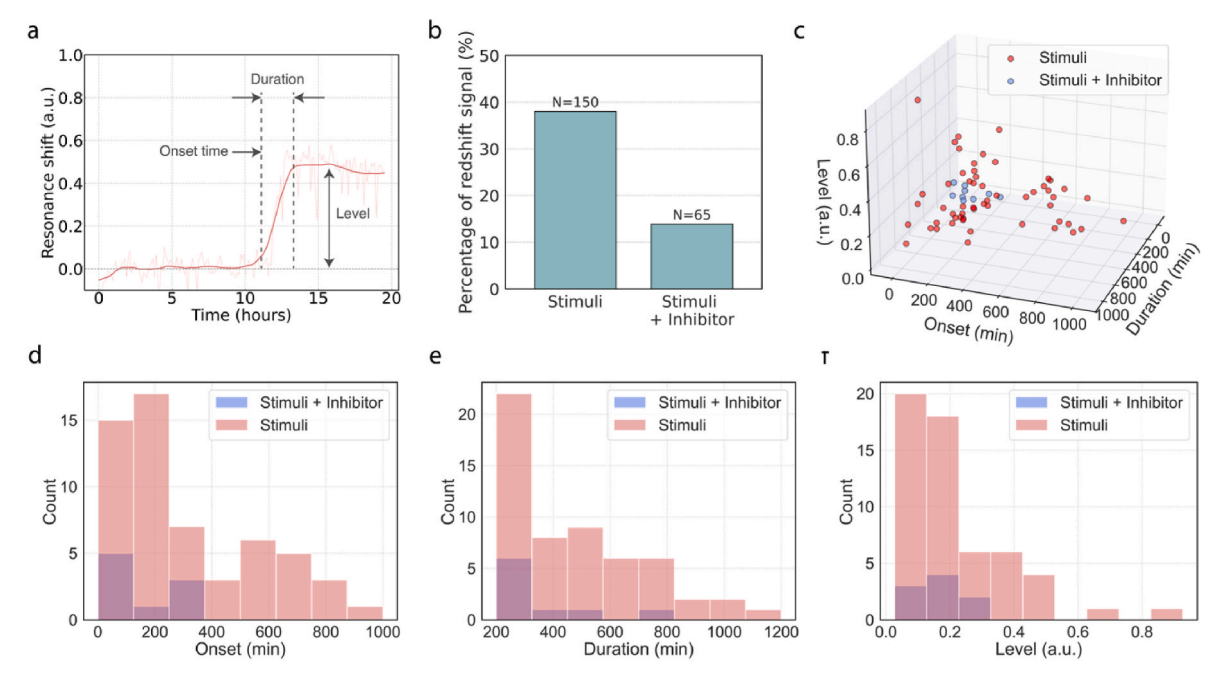


Fig. 5. Statistics of the IL-2 secretion from hundreds of EL4 cells. (a) Temporal sensorgram obtained from a single EL4 cell secreting IL-2 cytokine annotated with the definition of onset, duration, and level of secretion. (b) Percentage of single cells showing IL-2 secretion signal for both experimental group (with stimuli) and control group (with stimuli + inhibitor). N indicates the total numbers of the cells in each group. (c) 3D scatter plot of all secreting single EL4 cells with chemical stimuli and with stimuli and inhibitor. (d–f) Histogram of secretion onset time, duration, and level for the two cell groups.

longer period and reached higher signal levels. This can be again related to the heterogeneity of the cell response. In principle, the total secretion amount from a single cell can be correlated to the spectral shift data with the calibration curves. In our set-up, although the acquired shift signal is linked to the total amount, it is still partial because of the limited monitored area over each well by the slit.

#### 4. Conclusion

We introduced a novel platform based on nanoplasmonic microarray for real-time single-cell cytokine secretion analysis in high-throughput from a large number of single cells in a statistical way. The platform utilizes automated scanning over the microarray to acquire the spectroscopic and optical images simultaneously for tracking the spectral shift information and cell morphology and provides a comprehensive understanding of cellular behavior. Time-resolved 1D spectroscopic images were processed to construct a spatiotemporal sensorgram for a given cell to monitor the spatial distribution of secreted cytokine over long periods of time at high resolution. This biosensing platform enables cytokine secretion analysis from individual living single-cells in terms of various attributes that define the secretion behaviour such as onset time, duration and secretion amount and provide insights to the characterization and screening of single cells. The accessible microwell array part of the biochip used for cell isolation fulfills the potential of simple and efficient cell retrieval in the future. Algorithm-aided cell recognition for automated stage position and ROI assignment can also be potentially implemented to reduce manual handling process and reach a higher throughput. The unique features of our platform including highthroughput and real-time analysis capability, label-free operation and versatile configuration makes it an ideal system for fundamental cell studies and clinical research towards applications in diagnostics, personalized cell therapy and drug screening.

## CRediT authorship contribution statement

**Yen-Cheng Liu:** Conceptualization, Software, Validation, Formal analysis, Investigation, Writing – original draft, Writing – review &

editing, Visualization. Saeid Ansaryan: Validation, Investigation, Writing – review & editing. Xiaokang Li: Conceptualization, Validation, Writing – review & editing. Eduardo R. Arvelo: Conceptualization, Software, Writing – review & editing. Hatice Altug: Conceptualization, Validation, Writing – review & editing, Supervision, Project administration, Funding acquisition.

## Declaration of competing interest

The authors declare that they have no known competing financial interests or personal relationships that could have appeared to influence the work reported in this paper.

## Acknowledgments

The research leading to these results has received funding from the Société Académique Vaudoise supported by the Novartis Consumer Health Foundation, the ISREC-Biltema Foundation, European Union Horizon 2020 Framework Programme for Research and Innovation under Grant Agreement No. 7777214 (NOCTURNO), and the Taiwan EPFL PhD scholarship. The authors acknowledge École Polytechnique Fédérale de Lausanne (EPFL), Center of MicroNano Technology for nanofabrication, and Biological Electron Microscopy facility at EPFL for SEM imaging. The authors also thank Ophélie Berthuy and Guilhem Tourniaire from Cellenion for the support of single-cell spotting, and Léonard Equer for the assistance in improving the user interface of image acquisition and real-time analysis.

# Appendix A. Supplementary data

Supplementary data to this article can be found online at https://doi.org/10.1016/j.bios.2021.113955.

#### References

- Bithi, S.S., Vanapalli, S.A., 2017. Microfluidic cell isolation technology for drug testing of single tumor cells and their clusters. Sci. Rep. 7, 1–12. https://doi.org/10.1038/ srep.41707
- Brouzes, E., Medkova, M., Savenelli, N., Marran, D., Twardowski, M., Hutchison, J.B., Rothberg, J.M., Link, D.R., Perrimon, N., Samuels, M.L., 2009. Droplet microfluidic technology for single-cell high-throughput screening. Proc. Natl. Acad. Sci. U.S.A. 106, 14195–14200. https://doi.org/10.1073/pnas.0903542106.
- Bucheli, O.T.M., Sigvaldadóttir, I., Eyer, K., 2021. Measuring single-cell protein secretion in immunology: technologies, advances, and applications. Eur. J. Immunol. 51, 1334–1347. https://doi.org/10.1002/EJI.202048976.
- Carlo, D., Di, Wu, L.Y., Lee, L.P., 2006. Dynamic single cell culture array. Lab Chip 6, 1445–1449. https://doi.org/10.1039/b605937f.
- Chang, K., Pi, Y., Lu, W., Wang, F., Pan, F., Li, F., Jia, S., Shi, J., Deng, S., Chen, M., 2014. Label-free and high-sensitive detection of human breast cancer cells by aptamer-based leaky surface acoustic wave biosensor array. Biosens. Bioelectron. 60, 318–324. https://doi.org/10.1016/j.bios.2014.04.027.
- Dura, B., Dougan, S.K., Barisa, M., Hoehl, M.M., Lo, C.T., Ploegh, H.L., Voldman, J., 2015. Profiling lymphocyte interactions at the single-cell level by microfluidic cell pairing. Nat. Commun. 61 6, 1–13. https://doi.org/10.1038/ncomms6940, 2015.
  Farrar, J.J., Fuller-Farrar, J., Simon, P.L., Hilfiker, M.L., Stadler, B.M., Farrar, W.L.,
- Farrar, J.J., Fuller-Farrar, J., Simon, P.L., Hilfiker, M.L., Stadler, B.M., Farrar, W.L., 1980. Thymoma production of T cell growth factor (Interleukin 2). J. Immunol. 125.
- Gaster, R.S., Xu, L., Han, S.J., Wilson, R.J., Hall, D.A., Osterfeld, S.J., Yu, H., Wang, S.X., 2011. Quantification of protein interactions and solution transport using highdensity GMR sensor arrays. Nat. Nanotechnol. 6, 314–320. https://doi.org/10.1038/ nnano.2011.45.
- Han, Q., Bagheri, N., Bradshaw, E.M., Hafler, D.A., Lauffenburger, D.A., Love, J.C., 2012. Polyfunctional responses by human T cells result from sequential release of cytokines. Proc. Natl. Acad. Sci. U.S.A. 109, 1607–1612. https://doi.org/10.1073/ pnas.1117194109.
- Hartlmayr, D., Ctortecka, C., Seth, A., Mendjan, S., Tourniaire, G., Mechtler, K., 2021. An automated workflow for label-free and multiplexed single cell proteomics sample preparation at unprecedented sensitivity. bioRxiv 4 (14), 439828. https://doi.org/ 10.1101/2021.04.14.439828, 2021.
- Hsu, H.Y., Ohta, A.T., Chiou, P.Y., Jamshidi, A., Neale, S.L., Wu, M.C., 2010. Phototransistor-based optoelectronic tweezers for dynamic cell manipulation in cell culture media. Lab Chip 10, 165–172. https://doi.org/10.1039/b906593h.
- Juan-Colás, J., Hitchcock, I.S., Coles, M., Johnson, S., Krauss, T.F., 2018. Quantifying single-cell secretion in real time using resonant hyperspectral imaging. Proc. Natl. Acad. Sci. U.S.A. 115, 13204–13209. https://doi.org/10.1073/pnas.1814977115.
- Khansili, N., Rattu, G., Krishna, P.M., 2018. Label-free optical biosensors for food and biological sensor applications. Sensor. Actuator. B Chem. https://doi.org/10.1016/j. cpb. 2018 03 004
- Kimmerling, R.J., Lee Szeto, G., Li, J.W., Genshaft, A.S., Kazer, S.W., Payer, K.R., De Riba Borrajo, J., Blainey, P.C., Irvine, D.J., Shalek, A.K., Manalis, S.R., 2016. A microfluidic platform enabling single-cell RNA-seq of multigenerational lineages. Nat. Commun. 7, 1–7. https://doi.org/10.1038/ncomms10220.
- Länge, K., Bender, F., Voigt, A., Gao, H., Rapp, M., 2003. A surface acoustic wave biosensor concept with low flow cell volumes for label-free detection. Anal. Chem. 75, 5561–5566. https://doi.org/10.1021/ac0207574.
- Lawson, D.A., Kessenbrock, K., Davis, R.T., Pervolarakis, N., Werb, Z., 2018. Tumour heterogeneity and metastasis at single-cell resolution. Nat. Cell Biol. 20, 1349–1360. https://doi.org/10.1038/s41556-018-0236-7, 2018 2012.
- Li, X., Soler, M., Szydzik, C., Khoshmanesh, K., Schmidt, J., Coukos, G., Mitchell, A., Altug, H., 2018. Label-free optofluidic nanobiosensor enables real-time analysis of single-cell cytokine secretion. Small 14, 1800698. https://doi.org/10.1002/ smll.201800698
- Ma, C., Fan, R., Ahmad, H., Shi, Q., Comin-Anduix, B., Chodon, T., Koya, R.C., Liu, C.-C., Kwong, G.A., Radu, C.G., Ribas, A., Heath, J.R., 2011. A clinical microchip for evaluation of single immune cells reveals high functional heterogeneity in phenotypically similar T cells. https://doi.org/10.1038/nm.2375.
- Makridakis, M., Vlahou, A., 2010. Secretome proteomics for discovery of cancer biomarkers. J. Proteonomics. https://doi.org/10.1016/j.jprot.2010.07.001.
- Mazutis, L., Gilbert, J., Ung, W.L., Weitz, D.A., Griffiths, A.D., Heyman, J.A., 2013. Single-cell analysis and sorting using droplet-based microfluidics. Nat. Protoc. 8, 870–891. https://doi.org/10.1038/nprot.2013.046.
- Miyajima, C., Itoh, Y., Inoue, Y., Hayashi, H., 2015. Positive regulation of interleukin-2 expression by a pseudokinase, tribbles 1, in activated T cells. Biol. Pharm. Bull. 38, 1126–1133. https://doi.org/10.1248/BPB.B15-00002.

- Monticone, F., Alu, A., 2017. Metamaterial, plasmonic and nanophotonic devices. Rep. Prog. Phys. https://doi.org/10.1088/1361-6633/aa518f.
- Munn, D.H., Beall, A.C., Song, D., Wrenn, R.W., Throckmorton, D.C., 1995. Activation-induced apoptosis in human macrophages: developmental regulation of a novel cell death pathway by macrophage colony-stimulating factor and interferon gamma. J. Exp. Med. 181, 127–136. https://doi.org/10.1084/JEM.181.1.127.
- Olive, P.L., Aquino-Parsons, C., 2004. Measurement of tumor hypoxia using single-cell methods. Semin. Radiat. Oncol. 14, 241–248. https://doi.org/10.1016/J. SEMRADONC.2004.04.003.
- Pui, T.S., Kongsuphol, P., Arya, S.K., Bansal, T., 2013. Detection of tumor necrosis factor (TNF-α) in cell culture medium with label free electrochemical impedance spectroscopy. Sensor. Actuator. B Chem. 181, 494–500. https://doi.org/10.1016/j. snb.2013.02.019.
- Rettig, J.R., Folch, A., 2005. Large-scale single-cell trapping and imaging using microwell arrays. Anal. Chem. 77, 5628–5634. https://doi.org/10.1021/ac0505977.
- Schuerwegh, A.J., Stevens, W.J., Bridts, C.H., Clerck, L.S. De, 2001. Evaluation of monensin and brefeldin A for flow cytometric determination of interleukin-1 beta, interleukin-6, and tumor necrosis factor-alpha in monocytes. Cytometry 46, 172–176. https://doi.org/10.1002/CYTO.1102.
- Shin, S.R., Kilic, T., Zhang, Y.S., Avci, H., Hu, N., Kim, D., Branco, C., Aleman, J., Massa, S., Silvestri, A., Kang, J., Desalvo, A., Hussaini, M.A., Chae, S.K., Polini, A., Bhise, N., Hussain, M.A., Lee, H.Y., Dokmeci, M.R., Khademhosseini, A., 2017. Label-free and regenerative electrochemical microfluidic biosensors for continual monitoring of cell secretomes. Adv. Sci. 4 https://doi.org/10.1002/ advs.2016.00522
- Sojka, D.K., Bruniquel, D., Schwartz, R.H., Singh, N.J., 2004. IL-2 secretion by CD4+ T cells in vivo is rapid, transient, and influenced by TCR-specific competition. J. Immunol. 172, 6136–6143. https://doi.org/10.4049/JIMMUNOL.172.10.6136.
- Soler, M., Calvo-Lozano, O., Estevez, M.-C., Lechuga, L.M., 2020. Nanophotonic biosensors: driving personalized medicine. Opt Photon. News 31, 24. https://doi. org/10.1364/opn.31.4.000024.
- Taff, B.M., Voldman, J., 2005. A scalable addressable positive-dielectrophoretic cell-sorting array. Anal. Chem. 77, 7976–7983. https://doi.org/10.1021/ac0513616.
- Thurley, K., Wu, L.F., Altschuler, S.J., 2018. Modeling cell-to-cell communication networks using response-time distributions. Cell Syst 6, 355–367. https://doi.org/10.1016/J.CELS.2018.01.016 e5.
- Vallone, V.F., Telugu, N.S., Fischer, I., Miller, D., Schommer, S., Diecke, S., Stachelscheid, H., 2020. Methods for automated single cell isolation and sub-cloning of human pluripotent stem cells. Curr. Protoc. Stem Cell Biol. 55, e123. https://doi. org/10.1002/CPSC.123.
- Wang, D., Bodovitz, S., 2010. Single cell analysis: the new frontier in 'omics. Trends Biotechnol. 28, 281–290. https://doi.org/10.1016/J.TIBTECH.2010.03.002.
- Wesselborg, S., Janssen, O., Kabelitz, D., 1993. Induction of activation-driven death (apoptosis) in activated but not resting peripheral blood T cells. J. Immunol. 150.
- Wood, D.K., Weingeist, D.M., Bhatia, S.N., Engelward, B.P., 2010. Single cell trapping and DNA damage analysis using microwell arrays. Proc. Natl. Acad. Sci. U.S.A. 107, 10008–10013. https://doi.org/10.1073/pnas.1004056107.
- Wu, C., Chen, R., Liu, Y., Yu, Z., Jiang, Y., Cheng, X., 2017. A planar dielectrophoresis-based chip for high-throughput cell pairing. Lab Chip 17, 4008–4014. https://doi.org/10.1039/c7lc01082f.
- Wu, M.C., 2011. Optoelectronic Tweezers. Nat. Photonics. https://doi.org/10.1038/ pphoton.2011.98.
- Yesilkoy, F., Belushkin, A., Jahani, Y., Terborg, R., Li, X., Pruneri, V., Altug, H., 2019. Integrated nanophotonic biosensors for point-of care diagnostics and bioanalytical applications. In: 2019 Optical Fiber Communications Conference and Exhibition, OFC 2019 - Proceedings. Institute of Electrical and Electronics Engineers Inc. https://doi.org/10.1364/ofc.2019.m3d.4. Tu3D.4.
- Zanchetta, G., Lanfranco, R., Giavazzi, F., Bellini, T., Buscaglia, M., 2017. Emerging applications of label-free optical biosensors. Nanophotonics. https://doi.org/ 10.1515/nanoph-2016-0158.
- Zhou, Y., Shao, N., Bessa de Castro, R., Zhang, P., Ma, Y., Liu, X., Huang, F., Wang, R.F., Qin, L., 2020. Evaluation of single-cell cytokine secretion and cell-cell interactions with a hierarchical loading microwell chip. Cell Rep. 31, 107574. https://doi.org/ 10.1016/j.celrep.2020.107574.
- Zhu, C., Luo, X., Espulgar, W.V., Koyama, S., Kumanogoh, A., Saito, M., Takamatsu, H., Tamiya, E., 2020. Real-time monitoring and detection of single-cell level cytokine secretion using LSPR technology. Micromachines 11, 107. https://doi.org/10.3390/ mi11010107.